Photoabsorption spectra of cationic mercury clusters

Nicola Gaston and Peter Schwerdtfeger*
Centre of Theoretical Chemistry and Physics, Institute of Fundamental Sciences, Massey University (Auckland Campus), Private Bag 102904, North Shore MSC, Auckland, New Zealand

Bernd von Issendorff
Fakultät für Physik, Universität Freiburg, H. Herderstrasse 3, D-79104 Freiburg, Germany
(Received 8 March 2006; published 26 October 2006)

The experimental photoabsorption spectra of singly charged cationic mercury clusters (Hg_N^+) show a sharp change in behavior at cluster size $N=6$. Both relativistic density functional theory (DFT) and wave function based methods reveal that this corresponds to a structural change from linear to three-dimensional isomers. The simulated electronic excitation spectra obtained from time-dependent relativistic DFT agree well with the experimental results. Our quantum theoretical treatment confirms the change from single electron-hole excitations in small linear clusters to plasmonlike collective transitions for the larger three-dimensional clusters.

DOI: 10.1103/PhysRevA.74.043203 PACS number(s): 36.40.Wa, 31.15.Ar, 31.15.Ew, 31.25.−v

I. INTRODUCTION

Mercury is a particularly interesting case in cluster physics. The size dependence of its properties is most pronounced, due to a change from van der Waals (vdW) to more covalent and finally metallic bonding as the cluster size increases [1]. This transition is caused by the gap closing between the full 6*s* band and the empty 6*p* band, which is due to the increase of the width of both bands with increasing cluster size. Mercury clusters have therefore been the subject of a number of experimental and theoretical studies [1].

Experimentally mercury clusters have been characterized for example by measurements of the size dependence of photoionization potentials, innershell photoexcitation spectra, and cluster cohesive energies [2–4]. The results indicated a transition to metal behavior of the clusters in a size range between a few ten and a few hundred atoms, but it was difficult to make a clear statement at that time. A much more direct characterization of the nonmetal-to-metal transition was done recently by Cheshnovsky and co-workers, who have measured the width of the 6*s*-6*p* band gap as a function of the cluster size by photoelectron spectroscopy on size selected mercury cluster anions. They showed that the band gap closure (a necessary condition for metallic behavior) does not occur up to a size of 250 atoms, but can be extrapolated to a size of around 400 atoms [5]. Another experiment which showed the strong size dependence of the properties of mercury clusters was the measurement of photoabsorption cross section of size selected cluster cations [6,7], the interpretation of which is the subject of this paper.

The photoabsorption spectra of singly charged cations show distinctly different patterns in the size ranges of $N=3-6$ and $N=7-30$, as shown in Fig. 1. For small cluster sizes a weak absorption is observed at about 2 eV and a strong absorption band at 3–4 eV, both of which slightly shift to lower energies with increasing cluster size. Based on its strength and size dependence the strong excitation was tentatively assigned to be a $6s \rightarrow 6p$ transition [6]. Starting from about $N=5$ a second absorption is observed at higher energy, which eventually (at $N=7,8$) becomes dominant, as the low energy excitations vanish. This absorption is essentially size independent; from $N=5$ to the largest sizes studied it consists of one broad peak at about 5.75 eV. It has been interpreted as the onset of a plasmonlike resonance [6].

The measurement of the absorption spectra have been performed on positively charged clusters, as only for charged clusters it is possible to achieve the required size selectivity. One should note, however, that the positive charge can have a strong effect on the geometric and electronic structure of the clusters. Small neutral mercury clusters exhibit a large 6*s*-6*p* band gap and are dominantly van der Waals bound. They therefore tend to adopt Lennard-Jones type compact geometries like other van der Waals systems such as neutral rare gas clusters [8,9]. The positive charge changes the bonding type completely; it leads to increased covalent bonding as well as strong polarization interactions. In rare gas clusters the positive charge delocalizes over a linear chain of atoms (a trimer or tetramer), which is then covalently bound [10–14]. This core molecule is surrounded by neutral atoms bound by polarization forces; only further shells are mainly bound by van der Waals forces again. The positive charge also has a strong influence on the absorption properties of the rare gas clusters; additional to the normal high energy excitonic interband transition [15] a strong absorption band in the visible is observed, which is an intraband excitation made possible by the hole in the fully occupied valence band [16–18]. Because of the similarities between mercury and rare gas clusters one could therefore expect a similar behavior at least for the smallest mercury cluster cations.

On the theoretical side the size dependence of the bonding in neutral clusters has been studied by effective Hamiltonian methods [19] and quantum mechanical calculations [8,20]. The gradual change from van der Waals to covalent bonding occurs at small sizes, and even the mercury dimer has been shown to have important covalent contributions to the bonding [21]. Charged mercury clusters have been studied as well, both negatively [22] and positively charged [23–25]. In the latter case both the charge delocalization and its effect on

*Email address: p.a.schwerdtfeger@massey.ac.nz

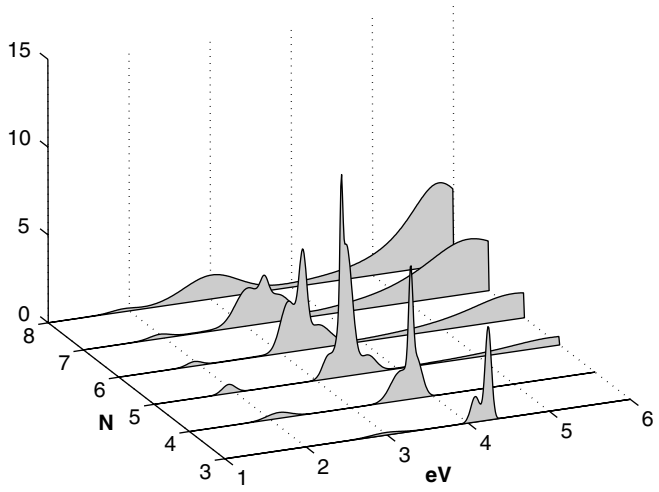

FIG. 1. The experimental photoabsorption spectra for Hg_N^+, $N=3-8$. Here fits to the original data [6,7] are shown.

the cluster structure as well as the resulting absorption properties have been examined by effective Hamiltonian methods. It was found that up to size five positively charged mercury clusters prefer linear structures, while larger clusters tend to be more compact. Here the charge was found to localize on a small triangular substructure [24]. This change in structure was accompanied by a change from "excitonic" to more "plasmonic" [23] characteristics of the absorption spectra. Accurate quantum theoretical calculations are not available, though. We therefore decided to investigate the photoabsorption spectra of small singly charged mercury clusters by both density functional theory and wave function based methods.

II. METHOD

The structures of the Hg cationic clusters were optimized [26] using density functional theory (DFT), both in the simple local spin density formalism (LSDA) [27,28] and using the more recent Perdew and Wang functional PW91 [29–31]. For comparison the structures up to $N=8$ were also optimized in second order perturbation theory (MBPT2) [26]. These were obtained as the lowest energy isomers of several optimized from different randomly selected starting configurations, and were confirmed as true minima by diagonalization of the mass-weighted force field. All calculations were performed using the scalar relativistic small-core Stuttgart pseudopotential for Hg [32] which produces excellent results for Hg_2 [33]. The basis set used for the geometry optimization was a correlation consistent set of $[6s5p4d1f]$ functions contracted to $(4s4p3d1f)$. For the electronic excitation calculations we optimized a slightly improved basis set to reproduce the atomic static polarizability for Hg, i.e., a $[7s6p4d2f]$ set contracted to $(5s5p3d2f)$. The minimum energy structures as obtained with LSDA, PW91, and MBPT2 are pictured in Fig. 2, along with selected low energy

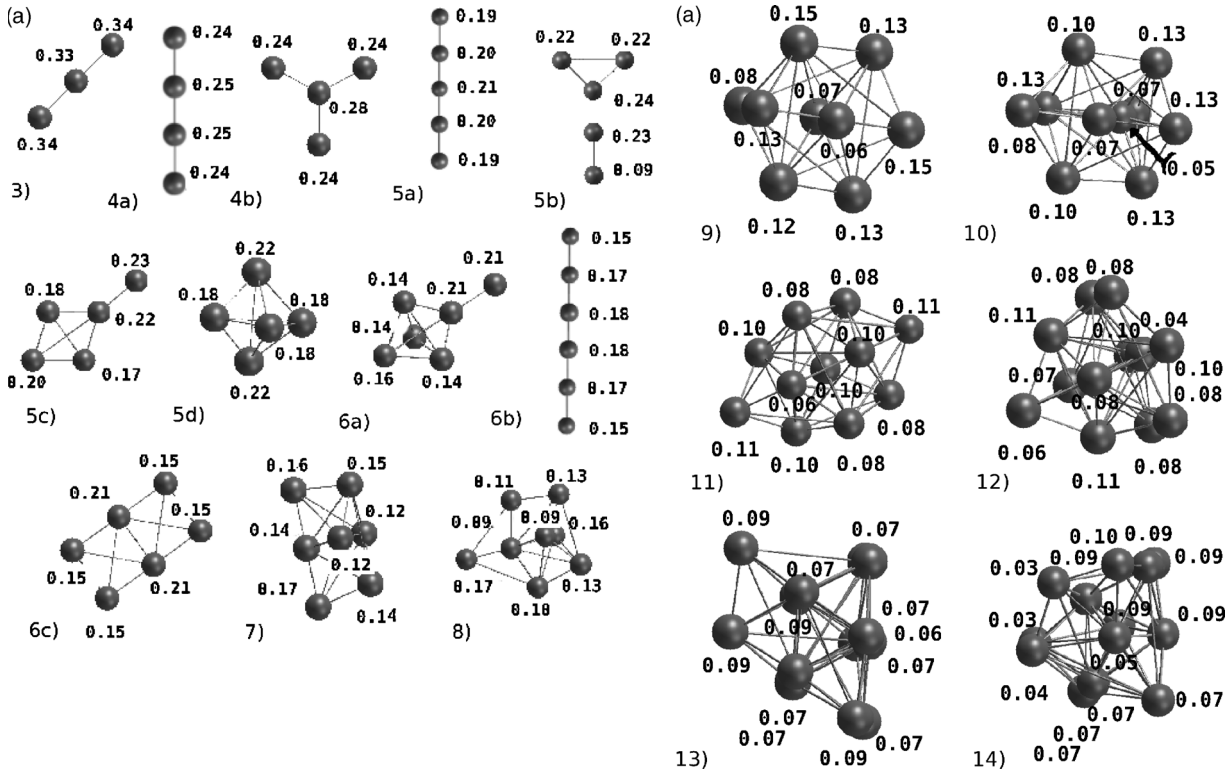

FIG. 2. The cation structures obtained with DFT (LSDA, PW91) and MBPT2. The numbers given are the Mulliken charges obtained in the PW91 calculation. For $N=6$ the global minimum depends on the method used. The linear structure is preferred by LSDA and PW91, but not by MBPT2, which prefers the 3D structure (6a). These structures are all very different to the Lennard-Jones type structures found for the neutral Hg clusters, although the larger sizes are similar to those found for charged Zn or Mg clusters [41–43].

isomers which are of interest. We note that introducing a positive charge increases the binding energy in Hg_n^+ substantially, for example from 0.05 eV for neutral Hg_2 to about 1.8 eV for Hg_2^+. Thus the long-range van der Waals part missed out in our density functional calculations is within the error limit in our procedure. Moreover, LDA overbinds substantially while PW91 underbinds slightly for neutral Hg clusters as pointed out previously. Thus, the correct binding energies are probably in-between the two density functional results.

At the optimized geometries electronic excited state calculations were obtained using configuration interaction calculations, both using the singles and perturbative doubles treatment as well as the symmetry adapted cluster configuration interaction (SAC-CI) program of Nakatsuji [26,34,35]. In addition we carried out time-dependent density functional calculations (TD-DFT) [36,37] which is more efficient in computer time and more suited for the larger cluster calculations. The accuracy of TD-DFT is critically depending on the exchange-correlation functional used [38]. Here we employ the Perdew-Burke-Ernzerhof (PBE) functional [39] for both the exchange and correlation part, which is known to give more reliable values for excited state calculations. The SAC-CI calculations [35] are a recent modification of the CI procedure. The inclusion of electron correlation for both the ground and excited electronic states is very important for the description of electronic excitations. The symmetry-adapted cluster expansion is defined

$$|\Psi_g\rangle = e^{\Sigma_i c_i s_i}|0\rangle \tag{1}$$

$$= \left(1 + \sum_i c_i s_i + \frac{1}{2}\sum_{i,j} c_i c_j s_i s_j + \cdots\right)|0\rangle, \tag{2}$$

where $|0\rangle$ is the ground state (closed shell) Hartree-Fock (HF) wave function and s_i is a symmetry-adapted excitation operator. These include both single and double excitations.

The SAC-CI wave function is then for excited or ionized states

$$|\Psi_e\rangle = \sum_k d_k|\Phi_k\rangle \tag{3}$$

$$= \left(\sum_k d_k R_k + \sum_{k,l} d_k c_l R_k s_l + \cdots\right)|0\rangle - \sum_k d_k s_{gk}|\Psi_g\rangle, \tag{4}$$

where

$$s_{gk} = \langle\Psi_g|R_k|\Psi_g\rangle. \tag{5}$$

The operators R_k are single and double excitation operators, and in the case of calculations on ionized species they will include the ionization operator. This implies that for SAC-CI calculations on the Hg_N^+ cations the SAC calculations are done on the neutral closed shell cluster, and in the subsequent CI calculations the cluster is ionized and the excited states are obtained subsequently. As this procedure is computationally most demanding, we were able to use it only for the smaller cluster sizes. For example, for $N=7$ and 8 only the TD-DFT and CIS calculations were performed, as even the CIS(D) calculations became prohibitively expensive. Both cluster coordinates and excitation energies are given in the supporting material [40].

III. RESULTS AND DISCUSSION

The optimized cluster structures are shown in Fig. 2. The PW91 and LSDA functionals give similar results for most clusters in this size range. As expected LSDA gives typically shorter bond lengths, but both methods find linear structures for the smallest sizes, and switch to three-dimensional (3D) structures as the number of atoms increases. Not surprisingly even for the smallest sizes the two methods disagree on the energetic sequence of the higher lying isomers.

MBPT2 turns out to prefer a transition to three dimensional structures at slightly smaller sizes; for $N=6$ LSDA and PW91 find the linear structure 6b to be more stable (Fig. 2), whereas MBPT2 switches to the three-dimensional structure 6a. From $N=7$ onwards, there is agreement at least that a three-dimensional structure is preferred. While the linear seven-atom cluster is still a local minimum on the hypersurface at the MBPT2 level of theory, it is 8 milli-hartree higher in energy than the corresponding three-dimensional structure. The same structural motifs are observed for all methods, although for the larger sizes we cannot fully exclude the possibility that the lowest energy structure found is not the global minimum. We mention that our structures for $N>5$ are not in agreement with the results of effective Hamiltonian calculations by Bennemann and co-workers [23,44].

MBPT2 calculations can be expected to yield the best results for small sizes. Indeed the calculated dissociation energies are in rather good agreement with experimental values; for Hg_2^+ and Hg_3^+ we get 1.41 and 2.19 eV, respectively, while photo-fragmentation experiments obtain 1.6 ± 0.2 eV and 2.42 ± 0.1 eV [45]. Because of the numerical effort MBPT2 has been used only up to size $N=8$, while the DFT optimizations have been performed up to $N=14$. In any case, as N increases and the system approaches the metallic state, single reference MBPT2 will eventually fail.

The variation of the (per atom) binding energies as a function of size for all three methods is shown in Fig. 3 and the corresponding values are listed in Table I. In the figure additionally three sets of experimental data as shown: binding energies as evaluated from the metastable decay of mercury clusters after electron impact ionization [4] and after photofragmentation [46] as well as from the measurement of the total kinetic energy release after photofragmentation [45]. For the first two data sets in the evaluation a binding energy of the ionized mercury dimer of 1.4 eV [47] was assumed, which is not in accordance with the later photofragmentation results. This causes an offset between the data sets for the small sizes. The theoretical values, especially the results of the MBPT2 calculations, reproduce the experimental values quite well. The transition to a three-dimensional structure at six atoms leads to a small step in the binding energy curve, which indicates a weakly bound sixth atom and is in agree-

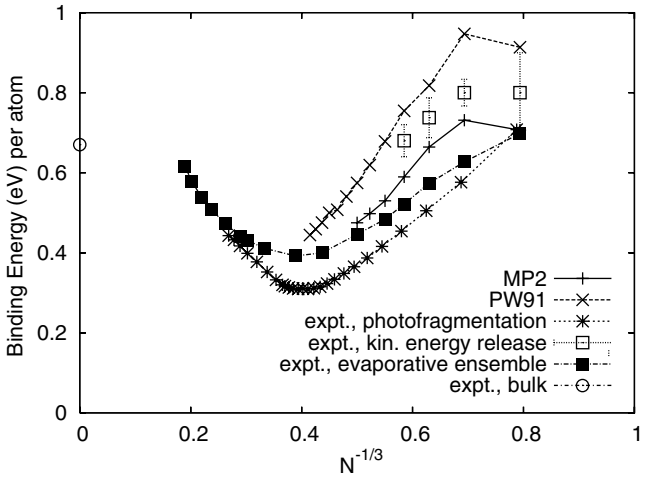

FIG. 3. Binding energies (per atom, ZPVE-corrected) of the cationic clusters. The structures are those of lowest energy for $N=2-14$, for which the calculated energies are given for PW91 and MBPT2. The experimental values have been obtained from the metastable decay of mercury clusters after electron impact ionization [4], from the metastable decay after photofragmentation [46], and from the measurement of the total kinetic energy release after photofragmentation [45].

ment with experimental mass spectra, where one sees a minimum in intensity at $N=6$ [3]. Obviously at this size neither the linear nor the three-dimensional structure are particularly stable (in contrast to the neutral clusters, where size $N=6$ is a magic number [8]). An interesting peculiarity of charged mercury clusters is evident from Fig. 3: the per atom dissociation energies decrease with cluster size and become significantly smaller than the bulk binding energy (0.67 eV or 0.025 hartree per atom [48]). This is in agreement with experiment, where it was found that the cohesive energy strongly decreases between size two and about size sixteen, and even drops below the finite surface corrected bulk value [4]. Only for larger sizes it increases towards the bulk value again. In contrast neutral mercury clusters exhibit a monotonous increase of the cohesive energy over the full size range starting from the weakly bound dimer [4,19]. This underlines the contrasting behavior of the charged and uncharged clusters. In the neutral clusters van der Waals (vdW) forces dominate for small sizes such that the per atom binding energy increases as the number of atoms is increased; the change in the bonding character towards covalent and eventually metallic additionally enhances the increase of bond strength with size. The cationic clusters show stronger ionic interactions dominating the cluster binding; by diluting the charge over a larger cluster these interactions become considerably weaker. One might imagine that this weakening of the ionic interaction would lead to an increase in the vdW character of the bond, even for the charged clusters, which could lead to a failure of DFT. However, even for the neutral clusters there is a significant covalent component of the bonding which increases with cluster size, so that DFT remains useful. The reasonable agreement between DFT (especially PW91) and the MBPT2 results would seem to confirm this. At a certain cluster size the onset of covalent/metallic bonding again enhances the interaction, but this occurs outside of the size range studied here.

TABLE I. A comparison of binding energies for the different isomers shown in Fig. 2. The labeling is as in Fig. 2. Binding energies are in a.u. and are given both with and without the zero-point vibrational energy (ZPVE) correction.

	Binding Energy+ZPVE			Binding Energy		
Isomer	LSDA	PW91	MBPT2	LSDA	PW91	MBPT2
2	−0.0787	−0.0669	−0.0519	−0.0789	−0.0671	−0.0522
3	−0.1272	−0.1039	−0.0806	−0.1277	−0.1044	−0.0812
4a	−0.1617	−0.1277	−0.0976	−0.1626	−0.1285	−0.0984
4b	−0.1512	−0.1196	−0.0923	−0.1521	−0.1202	−0.0929
5a	−0.1886	−0.1445	−0.1083	−0.1897	−0.1454	−0.1093
5b	−0.1809	−0.1378	−0.1060	−0.1820	−0.1387	−0.1069
5c	−0.1821	−0.1354	−0.1035	−0.1832	−0.1362	−0.1044
5d	−0.1820	−0.1305	−0.1029	−0.1831	−0.1313	−0.1038
6a	−0.2099	−0.1464	−0.1168	−0.2113	−0.1474	−0.1179
6b	−0.2107	−0.1570	−0.1153	−0.2122	−0.1581	−0.1165
6c	−0.2091	−0.1486	−0.1147	−0.2104	−0.1496	−0.1158
7	−0.2374	−0.1580	−0.1280	−0.2391	−0.1592	−0.1293
8	−0.2586	−0.1676	−0.1396	−0.2605	−0.1689	−0.1410
9	−0.2917	−0.1772		−0.2939	−0.1788	
10	−0.3078	−0.1849		−0.3103	−0.1865	
11	−0.3453	−0.2001		−0.3482	−0.2021	
12	−0.3730	−0.2075		−0.3762	−0.2096	
13	−0.3948	−0.2170		−0.3982	−0.2193	
14	−0.4261	−0.2261		−0.4300	−0.2286	

TABLE II. A comparison of excitation energies (in eV) for the different methods used for Hg_2^+. The oscillator strengths (f) are given as well as the symmetry of the excited electronic state (the ground state is $^2\Sigma_u^+$). The spin symmetry for all excited states is $S=1/2$. Only the first nine energies are listed.

	TD-DFT	f	Sym.	CIS	CIS(D)	f	Sym.	SAC-CI	f	Sym.
1	3.103	0.057	Σ_g^+	3.458	3.156	0.001	Σ_g^+	3.114	0.051	Σ_g^+
2	4.709	0.000	Π_u	4.254	4.692	0.000	Π_u	5.100	0.000	Π_u
3	4.929	0.000	Σ_u^+	4.872	5.121	1.033	Σ_g^+	5.852	1.012	Σ_g^+
4	5.085	0.001	Π_g	5.417	6.086	0.050	Π_g	6.475	0.000	Σ_u
5	5.246	0.000	Π_u	6.688	6.944	0.000	Σ_u^+	6.593	0.014	Π_g
6	5.267	0.553	Σ_g^+	7.379	7.578	0.594	Π_g	7.095	0.000	Π_u
7	5.354	0.000	Π_u	7.600	6.369	0.000	Σ_u^+	7.220	0.000	Π_u
8	5.831	0.000	Π_u	8.118	7.905	0.202	Π_g	7.534	0.000	Π_u
9	6.435	0.027	Π_g	8.155	6.318	0.111	Π_g	8.183	0.264	Σ_g^+

As mentioned in the Introduction, the distribution of the positive charge on the cluster can yield valuable information about its electronic structure. Here the calculations give some unexpected results. The charge distribution as obtained from a Mulliken analysis of the PW91 results is indicated in Fig. 2. For the sizes for which we have MBPT2 results, the results are not dissimilar, with a difference of 0.01–0.05 in the Mulliken charges. It turns out that for all sizes the charge delocalizes through all of the cluster atoms, which indicates an early onset of covalent bonding. This is even the case for Hg_3^+ where the charge is distributed perfectly equally over all three atoms (0.32:0.35:0.32 within MBPT2). This would not be possible if the orbital occupied by the positive charge had pure s character. In this case the orthogonality of the s-band orbitals requires a charge distribution of 1/4:1/2:1/4, as is seen in the rare gas trimer He_3^+, and in the positively charged heavier rare gas trimers where we have a hole in the σ_u orbital [12,49]. The equal distribution of the charge indicates a mixing with p-band states; indeed the calculation shows that the orbital occupied by the positive charge has 10% of p character. Obviously here the bond shortening induced by the positive charge strongly enhances the s-p hybridization. The same is true for the larger clusters; in no case does one observe the typical structure of charged van der Waals systems, with neutral atoms attached to an ionized core molecule. It seems that even for the outer atoms with low coordination numbers the weak bond contraction caused by the polarization interaction leads to enhanced s-p hybridization and therefore more covalent bonding, which then allows for a complete delocalization of the positive charge. It is an interesting question how large the particles have to be so that one can observe a localization of the charge solely on surface atoms, as one would expect for a metallic system. The sizes treated in this work in most cases consist only of surface atoms, so no answer to this question can be given here. It might even be the case that the clusters have to be of size $N>400$, which is the limit where the s-p band gap eventually closes and therefore "real" metal behavior sets in.

Another very peculiar property of mercury cluster cations is the preference for linear structures; up to $N=5$ the clusters definitely are linear, and the experimental results seem to indicate the existence of linear Hg_6^+ and maybe even of Hg_7^+. As already mentioned, these structures are found to be local minima in our MBPT2 calculations. For no other metallic (or rare gas) system are such structures observed. Being an s^2 metal, mercury can be expected to exhibit nondirectional bonding. This would lead to compact structures, as predicted for the neutral clusters [8]. The cations, however, prefer long chains. One reason could be the hybridization of the uppermost occupied orbitals with p-band σ-orbitals, which have a certain preference for directional charge delocalization, as is seen in charged rare gas tetramers [10–13]. Another reason could be the influence of relativity. It has been shown recently that gold clusters prefer planar geometries up to unusually large sizes [50–54]. It was furthermore demonstrated that this is directly related to scalar relativistic effects. As mercury seems to be the only divalent metal which adopts linear structures for sizes five and six, and is the only one experiencing strong relativistic effects, one might speculate that this is another case where the relativity causes the preference of low dimensional structures. Indeed, repeating the geometry optimization described above, but with the use of a nonrelativistic pseudopotential (otherwise analogous to the relativistic version, also obtained from the Stuttgart pseudopotential library along with the corresponding basis set) we find that for $N=3,4$, the linear structures are reproduced. However, this is not surprising, as linear Mg_3^+ and Mg_4^+ are also known to exist. For $N=5$ and 6, only a three-dimensional isomer was found in the nonrelativistic calculation, neither the linear structures nor the two-dimensional relativistic isomers being particularly stable. Thus the stability of these linear structures definitely is a relativistic effect as relativity enhances the 6s-6p separation, thus reducing covalent bonding. In the nonrelativistic case the 6s-6p hybridization is stronger from the start on. On the other hand, a positive charge in a bond (reduced occupation of the antibonding orbital) leads to bond shortening and thereby enhanced 6s-6p hybridization, thus the onset of covalent character and strongly enhanced binding energy. And third one has to take into account the relativistic bond contraction. It is this delicate interplay which determines whether the linear structure is preferred or not.

We will turn now to the cluster excitations. We start by briefly comparing the absorption spectra of Hg_2^+ obtained

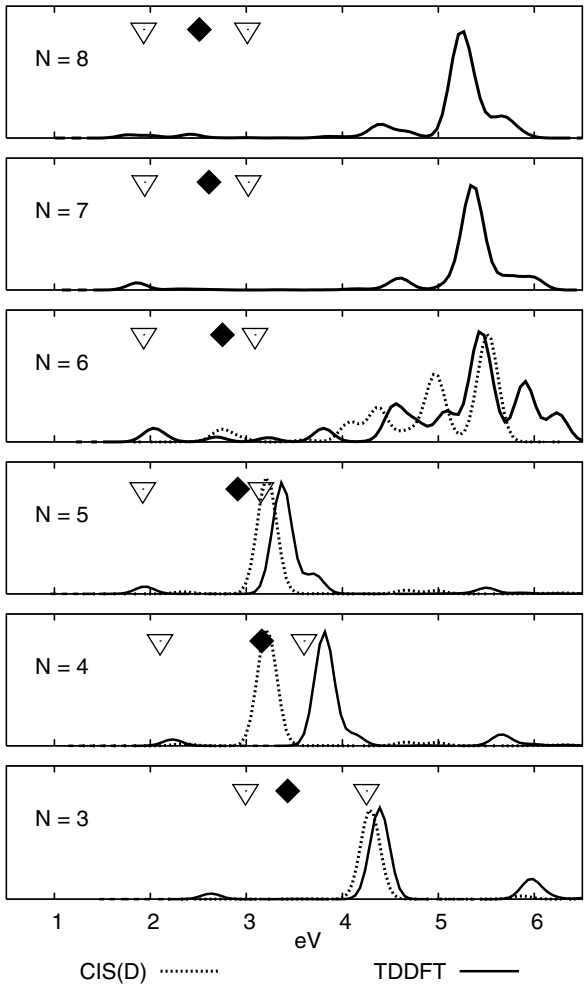

FIG. 4. The simulated spectra for Hg_N^+, $N=3-8$. The TD-DFT and CIS(D), ($N=3-6$) results are given. Y-axis units are scaled to the height of the maximum peak, to enable comparison between methods. The mean positions of the measured bands from experiment (Refs. [7,46]) are indicated with open triangles; the experimental band gap (measured for anions, taken from Table 1 of Ref. [5]) is marked by a closed diamond.

from CIS, CIS(D), SAC-CI, and TD-DFT calculations, Table II. The experimentally observed excitations are around 3 [45] and 5 eV [55]. The TD-DFT, CIS, CIS(D) and SAC-CI calculations reproduce both bands: they obtain a weak transition at 3.10, 3.46, 3.16, and 3.11 eV, respectively, and a strong transition (oscillator strength $f>0.5$) at 5.27, 4.87, 5.12, and 5.85 eV. Rather surprisingly, the SAC-CI energy is in poorest agreement with the experiment. In all cases the transition is to a $^2\Sigma_g^+$ state from the ground $^2\Sigma_u^+$ state, hence spin-orbit effects are expected to be relatively small. However, basis set effects are more important and we therefore used additional diffuse functions for all excited state calculations than what were contained in the basis set used for the structural optimization. The additional diffuse functions lower the excitation energy considerably and improve the calculated oscillator strengths.

All calculated excitation energies for the mercury clusters were based on the global minimum structures found in the MBPT2 calculations. Thus Hg_5^+ is assumed to be linear

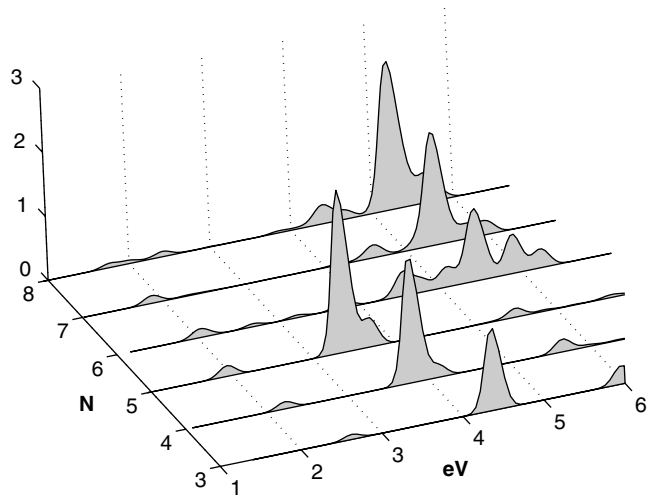

FIG. 5. The simulated TD-DFT spectra for Hg_N^+, $N=3-8$.

(structure 5a) and Hg_6^+ adopts a three-dimensional structure. The excitation energies were calculated for each size over the experimentally observed energy range (up to 6.0 eV). In order to simulate the measured spectra the line spectra obtained were broadened by Gaussians. The results of the CI and TD-DFT calculations are depicted in Fig. 4; the latter are shown as well in Fig. 5 which can be directly compared to the experimental results, see Fig. 1. The overall experimental observation of a shift from low to high energy absorptions at $N=5$ is reproduced nicely (despite the neglect of spin-orbit coupling which will change the excitation energies and more importantly the oscillator strengths), although the actual positions of the peaks are shifted by up to 1 eV. In general the agreement between TD-DFT, CIS(D) and the experimental spectra is consistently within 0.5 eV.

Both CIS and CIS(D) overestimate the lowest energy transition, for $N=3-6$. This error of 0.5–1.0 eV is due to the CI truncation and the neglect of spin-orbit coupling. However, the higher energy transitions are much more closely reproduced. For $N=3-5$, both CIS and CIS(D) find the second transition to much better accuracy. For $N=6$ the CIS(D) excitation energy is overestimated considerably, although the CIS calculation remains close to experiment.

The SAC-CI calculations were performed for the smallest sizes only to enable a comparison with the CIS(D) results. Many fewer low-energy states are found with the SAC-CI calculation. However, the lowest energy excitation (between 2–3 eV) is more accurately reproduced in the SAC-CI excitations. Unfortunately, the overall accuracy is less as the second excitation is not reproduced as well as with CIS(D). We therefore do not show the SAC-CI energies for $N>2$.

A comparison of the CIS calculations for the different isomers for $N=5$ and $N=6$ sheds some light on the question as to what degree the change in the spectra is structure dependent. From the comparison for Hg_5^+ [40] it does seem that the planar isomers give quite similar results to the linear ones for the excitation energies with appreciable oscillator strengths, when compared to the three-dimensional isomer. For both $N=5$ and 6 the linear and planar isomers have stronger (large oscillator strength) low energy transitions

compared to the three-dimensional isomers. In particular the three-dimensional isomer for $N=5$ has no low energy excitations with appreciable oscillator strength. Therefore while no isomer reproduces all experimentally observed transitions accurately, there is a clear correlation between the shift to three-dimensional structures seen for these sizes, and the experimentally observed disappearance of the strong low energy (3–4 eV) absorption band.

An analysis of the states contributing to the low energy transitions supports the earlier tentative assignment of these excitations. Of course the rather strong hybridization present even in the smallest sizes leads to appreciable mixing of single electron-hole excitations. Nevertheless, for all of the linear isomers (up to $N=6$) the general picture can be described as follows. There is the weak lowest energy transition, which shifts with increasing size from around 3 to 2 eV; this transition has dominant $6s \rightarrow 6s$ character, with the strongest contribution (60–70 %) from the excitation of an electron from the highest doubly occupied to the singly occupied molecular orbital (HOMO-1 $\rightarrow$ HOMO of the neutral cluster). This band therefore is the analogue of the absorption band seen in positively charged rare gas clusters. The strong absorption band at higher energy (3–4 eV), on the other hand, consists dominantly of an intraband ($6s \rightarrow 6p$) transition. For the slightly larger sizes ($N=4-6$) at the same energy another $6s \rightarrow 6s$ intraband transition appears, which is mainly an excitation from the third highest doubly occupied to the singly occupied molecular orbital. At the highest energy (4–6 eV) some weak transitions are found as well; these are again $6s \rightarrow 6p$ transitions with some admixture of $6s \rightarrow 6s$ transitions as well as excitations of *d*-band electrons.

This assignment of the main two absorptions of the small clusters as being dominantly an $6s \rightarrow 6s$ and an $6s \rightarrow 6p$ excitation is supported by the size dependence of the band gap of the clusters. In Fig. 4 additionally to the experimentally determined positions of the two bands the width of the $6s$-$6p$ band gap is shown, as determined by photoelectron spectroscopy on the cluster anions [5]. This demonstrates that the lowest excitation has an energy smaller than the band gap, which means that it can only be an interband transition. The strong absorption, on the other hand, has an energy slightly larger than the band gap, as can be expected for an interband transition. Note that the band gap shown is the lowest possible excitation energy of neutral mercury clusters in the anion geometry. Mercury cluster anions most probably do not adopt the linear structure of the cations, but more compact configurations [22]; the higher average coordination number in this case leads to reduction of the band gap. So one can expect the *s*-*p* band gap of the linear cluster cations to be slightly larger than the values shown, which is in even better agreement with the simple interpretation of the absorption bands.

For the three-dimensional clusters the picture becomes immediately different. A low energy transition at about 2 eV is still observed for Hg_6^+, with the doubly occupied $\rightarrow$ singly occupied ($6s \rightarrow 6s$) excitation being the dominant contribution. But all transitions thereafter have a much more correlated nature, which is evident in the number of contributing orbitals. This is typically larger than ten pairs for the higher energy excitations, so the one-electron picture starts to become obsolete. In the linear Hg_6^+ isomer for example there are four transitions found below 6 eV, which have between two and five contributing pairs of orbitals; 3D Hg_6^+ has eleven transitions with up to eighteen contributing pairs.

One can summarize this analysis in the following way: the smallest clusters exhibit two main absorption bands, one weak band of intraband transitions at low energy, which are made possible by the hole in the fully occupied *s* band, and a strong band of $6s \rightarrow 6p$ interband transitions at medium energy, which would be possible in the neutral clusters as well (position and strength could of course be quite different). For larger, three-dimensional clusters a band of highly correlated transitions at high energies dominates, which can be seen as the precursor of the plasmon excitation in bulklike mercury particles.

Because the absorption spectra in the size range $N=5-7$ show both low energy (size dependent) and high energy (plasmonlike) features, it raises the question of whether both types of isomers, linear and three-dimensional, are present in the experiment. Conversely, a more indirect correlation between structure and absorption spectra may exist.

IV. CONCLUSIONS

The optimized cationic clusters show a clear structural transition at precisely the sizes at which the experimental shift from a low ($6s \rightarrow 6sp$) to a high energy transition was observed. The emergence of the plasmonlike size-independent absorption at $N=5-7$ correlates exactly with the first appearance of a low lying three-dimensional isomer ($N=5$) and the disappearance of a low lying linear isomer ($N=7$). The CIS, CIS(D), TD-DFT, and SAC-CI calculations performed reproduce some aspects of the experiment clearly, but not all. Reasonable agreement is seen between the different methods used, although the quality of the SAC-CI results is less than expected. In particular, it is difficult to determine whether the combination of low and high energy absorptions between $N=5-7$ is due to the presence of multiple (both linear or planar, and 3D) isomers, or whether the calculated absorption spectra of certain isomers are still not sufficiently accurate. Nevertheless the results indicate that the shift to more compact three-dimensional structures corresponds to increasing metallicity and $6p$ hybridization in the cluster; and therefore it is the interplay between the electronic and geometrical properties of the cluster that causes the change in the experimental spectra.

The variation between the calculated and experimental excitation energies is quite large; this is not surprising when the CIS(D) corrections can shift the CIS energies considerably, often by 0.5 eV and up to 0.8 eV. The TD-DFT calculations are consistent with CIS(D), but in general closer to

the experiment. It remains a nontrivial task to simulate accurately the absorption spectra of heavy metal clusters such as the Hg_N^+ clusters here.

ACKNOWLEDGMENTS

N. G. is grateful for support from TEC. Support by the Marsden Fund (Wellington) is gratefully acknowledged.

[1] G. M. Pastor and K. H. Bennemann, in *Clusters of Atoms and Molecules I*, edited by H. Haberland (Springer-Verlag, Berlin, 1995), p. 86.
[2] C. Bréchignac, M. Broyer, P. Cahuzac, G. Delacretaz, P. Labastie, J. P. Wolf, and L. Wöste, Phys. Rev. Lett. **60**, 275 (1988).
[3] K. Rademann, B. Kaiser, U. Even, and F. Hensel, Phys. Rev. Lett. **59**, 2319 (1987).
[4] H. Haberland, H. Kornmeier, H. Langosch, M. Oschwald, and G. Tanner, J. Chem. Soc., Faraday Trans. **86**, 2473 (1990).
[5] R. Busani, M. Folkers, and O. Cheshnovsky, Phys. Rev. Lett. **81**, 3836 (1998).
[6] H. Haberland, B. von Issendorff, J. Yufeng, and T. Kolar, Phys. Rev. Lett. **69**, 3212 (1992).
[7] H. Haberland, B. von Issendorff, J. Yufeng, T. Kolar, and G. Thanner, Z. Phys. D: At., Mol. Clusters **26**, 8 (1993).
[8] G. E. Moyano, R. Wesendrup, T. Söhnel, and P. Schwerdtfeger, Phys. Rev. Lett. **89**, 103401 (2002).
[9] P. Schwerdtfeger, N. Gaston, R. P. Krawczyk, R. Tonner, and G. E. Moyano, Phys. Rev. B **73**, 064112 (2006).
[10] T. Ikegami, T. Kondow, and S. Iwata, J. Chem. Phys. **98**, 3038 (1993).
[11] M. Amarouche, G. Durand, and J. P. Malrieu, J. Chem. Phys. **88**, 1010 (1988).
[12] P. J. Kuntz and J. Valldorf, Z. Phys. D: At., Mol. Clusters **8**, 195 (1988).
[13] B. v. Issendorff, A. Hofmann, and H. Haberland, J. Chem. Phys. **111**, 2513 (1999).
[14] H. Haberland, Surf. Sci. **156**, 305 (1985).
[15] J. Stapelfeldt, J. Wörmer, and Th. Möller, Phys. Rev. Lett. **62**, 98 (1989).
[16] N. E. Levinger, D. Ray, and W. C. Lineberger, J. Chem. Phys. **89**, 5654 (1988).
[17] H. Haberland, B. von Issendorff, Th. Kolar, H. Kornmeier, C. Ludewigt, and A. Risch, Phys. Rev. Lett. **67**, 3290 (1991).
[18] J. A. Gascon, R. W. Hall, C. Ludewigt, and H. Haberland, J. Chem. Phys. **117**, 8391 (2002).
[19] M. E. Garcia, G. M. Pastor, and K. H. Bennemann, Phys. Rev. Lett. **67**, 1142 (1991).
[20] M. Dolg and H.-J. Flad, Mol. Phys. **91**, 815 (1997).
[21] P. Schwerdtfeger, J. Li, and P. Pyykkö, Theor. Chim. Acta **87**, 313 (1994).
[22] Y. Wang, H.-J. Flad, and M. Dolg, Int. J. Mass. Spectrom. **201**, 197 (1999).
[23] S. Grabowski, M. E. Garcia, and K. H. Bennemann, Phys. Rev. Lett. **72**, 3969 (1998).
[24] M. E. Garcia, G. M. Pastor, and K. H. Bennemann, Phys. Rev. B **48**, 8388 (1993).
[25] F. Joyes and R. J. Tarento, J. Phys. (France) **50**, 2673 (1989).
[26] M. J. Frisch, *et al.* Gaussian 03, Revision B.03 (Gaussian, Inc., Pittsburgh PA, 2003).
[27] P. A. M. Dirac, Cambridge Philos. Soc. **26**, 376 (1930).
[28] S. J. Vosko, L. Wilk, and M. Nusair, Can. J. Phys. **58**, 1200 (1980).
[29] Y. Wang and J. P. Perdew, Phys. Rev. B **43**, 8911 (1991).
[30] Y. Wang and J. P. Perdew, Phys. Rev. B **44**, 13298 (1991).
[31] J. P. Perdew and Y. Wang, Phys. Rev. B **45**, 13244 (1992).
[32] D. Andrae, U. Haeussermann, M. Dolg, H. Stoll, and H. Preuss, Theor. Chim. Acta **77**, 123 (1990).
[33] P. Schwerdtfeger, R. Wesendrup, G. Moyano, A. Sadlej, J. Greif, and F. Hensel, J. Chem. Phys. **115**, 7401 (2001).
[34] M. Head-Gordon, R. J. Rico, M. Oumi, and T. J. Lee, Chem. Phys. Lett. **219**, 21 (1994).
[35] H. Nakatsuji, M. Hada, M. Ehara, K. Toyota, R. Fukuda, J. Hasegawa, M. Ishida, T. Nakajima, Y. Honda, O. Kitao, and H. Nakai, SAC/SAC-CI Program, Department of Synthetic Chemistry and Biological Chemistry, Graduate School of Engineering, Kyoto University, Japan, 2002.
[36] E. Runge and E. K. U. Gross, Phys. Rev. Lett. **52**, 997 (1984).
[37] E. K. U. Gross and W. Kohn, Phys. Rev. Lett. **55**, 2850 (1985).
[38] M. E. Casida, C. Jamorski, K. C. Casida, and D. R. Salahub, J. Chem. Phys. **108**, 4439 (1998).
[39] J. P. Perdew, K. Burke, and M. Ernzerhof, Phys. Rev. Lett. **77**, 3865 (1996).
[40] See EPAPS Document No. E-PLRAAN-74-066610 for MBPT2 cluster coordinates, TD-PBE excitation energies, and CIS excitation energies and oscillator strengths. For more information on EPAPS, see http://www.aip.org/pubservs/epaps.html.
[41] J. Akola, K. Rytkönen, and M. Manninen, Eur. Phys. J. D **16**, 21 (2001).
[42] J. Jellinek and P. H. Acioli, J. Phys. Chem. A **106**, 10919 (2002).
[43] N. Gaston and B. v. Issendorf (unpublished).
[44] M. E. Garcia, D. Reichardt, and K. H. Bennemann, J. Chem. Phys. **109**, 1101 (1998).
[45] B. v. Issendorff, Ph.D. thesis, Albert-Ludwigs-Universität, 1994.
[46] Th. Kolar, Ph.D. thesis, Albert-Ludwigs-Universität, 1993 (unpublished).
[47] S. H. Linn, C. L. Liao, J. M. Brown, and C. Y. Ng, Chem. Phys. Lett. **105**, 645 (1984).
[48] *The CRC Handbook of Chemistry and Physics*, edited by D. R. Lide (CRC Press, New York, 2006).
[49] H. Haberland, A. Hofmann, and B. v. Issendorff, J. Chem. Phys. **103**, 3450 (1999).
[50] F. Furche, R. Ahlrichs, P. Weis, C. Jacob, S. Gilb, T. Bierweiler, and M. K. Kappes, J. Chem. Phys. **117**, 6982 (2002).
[51] H. Häkkinen, M. Moseler, and U. Landman, Phys. Rev. Lett. **89**, 033401 (2002).

[52] H. Häkkinen, B. Yoon, U. Landman, X. Li, H.-J. Zhai, and L.-S. Wang, J. Phys. Chem. A **107**, 6168 (2003).

[53] S. Gilb, P. Weis, F. Furche, R. Ahlrichs, and M. M. Kappes, J. Chem. Phys. **116**, 4094 (2002).

[54] E. M. Férnandez, J. M. Soler, I. L. Garzón, and L. C. Balbás, Phys. Rev. B **70**, 165403 (2004).

[55] K. P. Huber and G. Herzberg, *Molecular Spectra and Molecular Structure IV* (Van Nostrand-Reinhold, New York, 1979).